ELSEVIER

Polymer 40 (1999) 4345–4352

polymer

The fine structure of metallocene-based linear polyethylenes: Part 1. A model grounded on molecular mobility

A. Alizadeh[a], A. Muñoz-Escalona[b], P. Lafuente[b], J.V. Garcia Ramos[a], J. Martínez-Salazar[a,*]

[a]*Instituto de Estructura de la Materia, CSIC, Serrano 119, 28006 Madrid, Spain*
[b]*Repsol I + D, Embajadores 183, 28045 Madrid, Spain*

Received 3 February 1998; accepted 22 August 1998

Abstract

A variety of techniques is used to describe the fine structure of a series of well defined linear polyethylenes, polymerized using the new generation of metallocene-based catalysts. The sample's molecular weight (M_w) is restricted to the usual values of processability of this material ranging from 14 K to 460 K. It will be clearly shown that the overall enthalpy of the rapidly crystallized samples follows a linear decrease with the log of M_w. The relative amounts of the different phases as seen from Raman spectroscopy and small angle X-ray scattering are evaluated as a function of molecular weight. As a consequence of the overall study, the contributions of the ordered and disordered regions to the long period are clearly separated and a semi-empirical expression for this essential structural parameter is proposed.

Keywords: Linear polyethylene; Fine structure; Metallocene-based catalysts

1. Introduction

The recent discovery of metallocene-based catalysts for the polymerization of the α-olefins has opened the possibility of synthesizing new materials with an efficient control of streoregularities, molecular weight (M_w) and molecular weight distribution, as well as comonomer incorporation [1]. One of the most important aspects in which homogeneous olefin polymerization by metallocene catalysts differs from the traditional heterogeneous Ziegler–Natta catalysis is that the resulting polymer chains follow the most probable M_w Flory–Schultz distribution [2], characteristic of this single type of metal centre catalysts with a well defined coordination environment. At the same time, a sufficient amount of the material, necessary for a suitable determination of the rheological and mechanical properties, can be obtained. The aim of this work is to describe in detail the microstructural parameters of a series of metallocene-based polyethylenes (PEM) covering a wide range of M_w, with distribution close to 2. In order to enhance the role of the molecular length upon the solidified structure a fast crystallization method was chosen.

The simplest and most widely accepted view is that the microstructure of melt-crystallized polyethylene (PE) consists of an alternation of more or less well ordered lamellar crystals separated by liquid-like domains (two-phase model), an idea which comes from both the lamellar nature of the folded single crystals and the characteristic X-ray diffraction patterns of semi-crystalline polymers [3]. However, this ideal two-phase model faced from the very beginning the difficulties associated with the drastic change of densities from 1 gcm^{-3} at the crystal core [4] to approximately 0.853 gcm^{-3} corresponding to the amorphous phase [5]. Thus, several approaches were suggested to solve the problem [6,7] having in common the idea of introducing an intermediate region of order. Assuming, then, the need of an interphase, the remaining question to answer nowadays is how extensive and relevant this interphase is compared to the overall structure. The development of the Raman spectroscopy applied to polymers allowed Strobl et al. [8] to quantify the fraction of material involved in the interfacial region. More recently, in a following and more thoroughly spectroscopic study, Mutter et al. [9] suggested that the amorphous region is formed itself by a pure liquid-like region and a transition region defined by a conformational state which is significantly different from the pure melt. Using NMR Cheng et al. [10] have also quantified the amount of interfacial material in PE in good agreement with Raman results. The final picture is then a two-phase system, each phase having a well distinguished interphase. In the present work the four-phase model for the structural characterization of the PE samples has been assumed.

* Corresponding author.

0032-3861/99/$ - see front matter
PII: S0032-3861(98)00654-5

Table 1
Sample name, weight-average molecular weight, M_w, polydispersity, M_w/M_n and total concentration of chain ends

Sample	M_w (g mol^{-1})	M_w/M_n	(CH_3/1000°C)
460 K	460 000	2.3	< 0.20
255 K	255 000	2.90	< 0.40
181 K	181 000	2.90	0.39
64 K	64 000	3.50	1.44
14 K	14 000	2.30	6.65

2. Materials and methods

The samples were prepared by Repsol I + D, following the Kaminsky method [11], where Cp_2ZrCl_2 has been employed as single side metallocene catalyst. Molecular parameters of these experimental PEM samples are listed in Table 1. It is of interest to point out that the PEM contain not short chain branching. Additionally, the molecular weight distribution is fairly symmetrical around the maximum (see Fig. 1). These two distinct features could be relevant to explain the remarkable homogeneous behaviour of these samples. Due to a lack of small angle X-ray scattering (SAXS) data, sample 460 K was only analysed by calorimetric methods.

The samples were compression moulded into films of 0.5 mm thick at 160°C and 150 bars and then rapidly crystallized between cold metallic plates. The melting behaviour of the samples has been studied by means of a Perkin–Elmer DSC-7. Similar discoid samples of 100 μm thickness and weight of 2.4 mg were used. To detect any reorganization of the crystals during heating on the dsc, the various melting endotherms were recorded at heating rates of 10, 20 and 40°C min^{-1}. Indium was used for temperature and specific heat calibration of the instrument. Since enthalpy values are not affected by heat transfer, corrections for sample thermal lag were not considered [12].

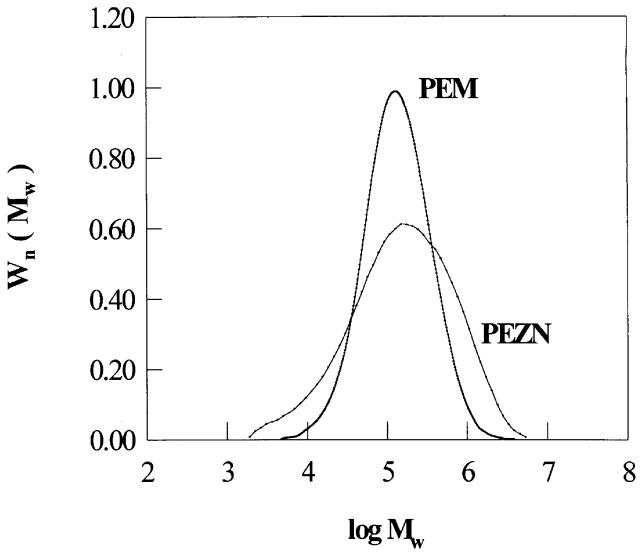

Fig. 1. Molecular weight distribution of a PE synthesized with metallocene catalysts as compared to a conventional Ziegler–Natta PE.

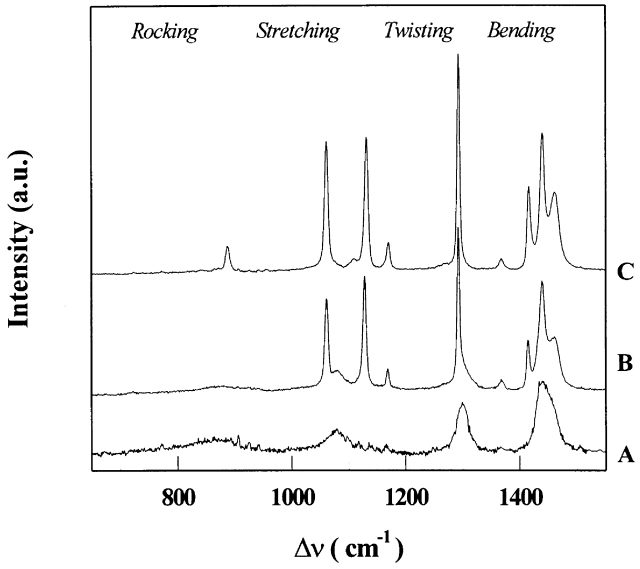

Fig. 2. Raman spectral region showing the internal modes of vibration in PE: (a) amorphous state, (b) semi-crystalline state, and (c) crystalline state.

Small angle X-ray scattering experiments were carried out by means of a Rigaku camera attached to a Rigaku rotating Cu anode operating at 40 kV and 140 mA. Pinhole collimation and photographic detection have been employed. One dimensional SAXS intensity plots were read on a Perkin–Elmer two dimensional microdensitometer with a pixel size of 50 μm. The scattered intensities at different angles were obtained by averaging six diametrical readings through the centre of the main beam position. The absorption coefficient of each sample, $\mu(\lambda = 1.5418$ Å), was measured in order to correct the experimental curves from primary beam and blind scattering effects. The average value of the long period L was calculated from the maximum of each Lorentz corrected SAXS curve by direct application of Bragg's law.

Macroscopic densities were measured at room temperature using the flotation method in a toluene/dioxane solution.

2.1. Raman spectroscopy

Raman spectroscopy was performed at room temperature using a Jobin–Yvon U1000 laser Raman spectrometer. A softly focused Argon ion laser (300 μm spot diameter) with an incident power of 300–400 mW has been employed. In each case five scans were recorded and the spectral resolution was about 2 cm^{-1}.

Following the procedure proposed by Mutter et al. [9], the mass fraction of the different phases in PEM can be calculated from the observed intensities in the internal mode region of the Raman spectrum (600–1600 cm^{-1}). In Fig. 2 this particular region of the solid paraffin, $C_{28}H_{58}$ spectrum

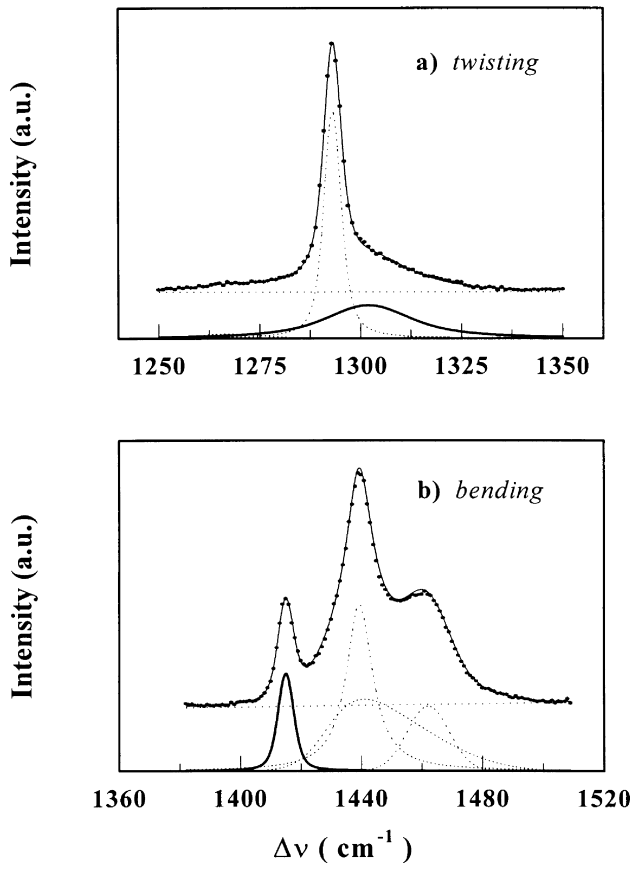

Fig. 3. Fitting of the twisting and bending Raman bands of PE using Voigt functions.

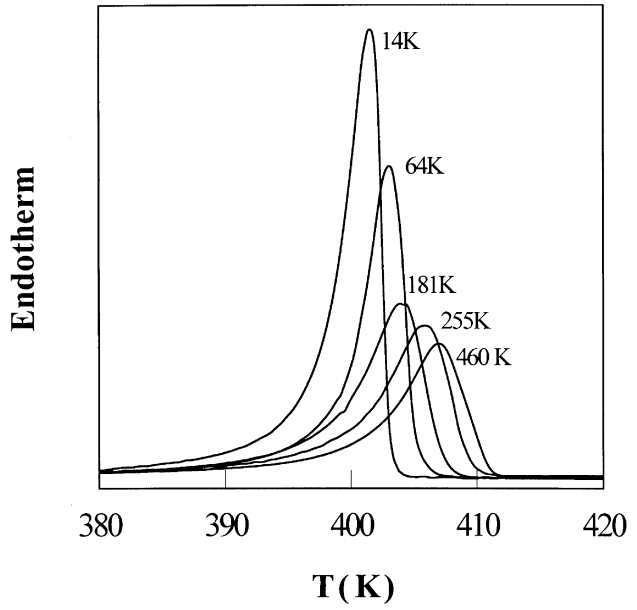

Fig. 4. DSC traces of PEM with different M_w.

taken at 25°C and the region of the PE spectra taken at 25°C and at 160°C, respectively, are compared. The four main vibrational modes—rocking, stretching, twisting and bending—are indicated in the figure. It has been demonstrated that the total intensity of the twisting vibrational mode (1250–1350 cm^{-1}) is independent of the state of order of the polymer [8]. Hence, it provides us with an internal standard. The intensities in Fig. 2 have been normalized with respect to the total intensity of the twisting vibrational range. The mass fraction of the orthorhombic crystals, α_c, can be derived by the intensity of the CH_2 bending band at 1416 cm^{-1}:

$$\alpha_c = \frac{I_{1416}/I_{tws}}{I_{1416}^{\alpha=1}/I_{tws}} \text{ where } I_{1416}^{\alpha=1}/I_{tws} = 0.493 \quad (1)$$

Similarly, the mass fraction of the whole amorphous regions, α_a, can be estimated from the CH_2 twisting vibrations according to:

$$\alpha_a = \frac{I_{1303}}{I_{tws}} \quad (2)$$

As suggested by these authors, the amorphous phase itself consists out of two main parts, a liquid-like region (α_l) and a transition region (α_{i-1}) where the chains exhibit a conformational state which is different from that of the pure melt. In the twisting region both amorphous domains contribute to the intensity of 1303 cm^{-1} band. However, only the pure liquid-like domain contributes to the rocking vibrational mode of the spectrum. The mass fraction of the liquid amorphous regions is calculated from the CH_2 rocking vibrations:

$$\alpha_l = \frac{I_{rock}(T)}{I_{rock}(T = 160)} \quad (3)$$

where T is the actual experimental temperature. Since α_l is always smaller than α_a, the difference $\alpha_{i-1} = \alpha_a - \alpha_l$ corresponds to the interfacial amorphous region. Finally, the mass fraction of the crystalline interfacial phase, i.e. regions where the chains adopt all-trans conformations but have lost their lateral order, can be deduced from the following relation:

$$\alpha_{i-c} = 1 - (\alpha_c + \alpha_a) \quad (4)$$

To calculate the integrated intensity of each band, a constant background, which accounts for the fluorescence intensity of the sample, was first subtracted from the experimental spectrum. Then the spectrum of the melt was scaled to that of the partially crystalline sample by means of the following expression: $A(\mu) = fM(\mu)$, where f is a weight factor and $M(\mu)$ is the spectrum of the melt. Finally, Voigt functions were used for the fitting of the experimental bands. In Fig. 3 the fitting procedure used in the twisting and bending regions for one of the PE samples is illustrated.

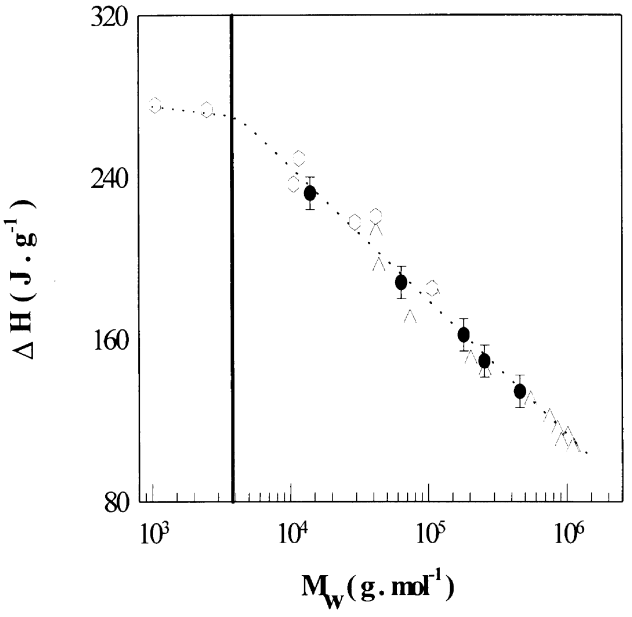

Fig. 5. Variation of the total enthalpy of PE with the log of M_w.

3. Results and discussion

We will present the results in two sections. In the first part we will analyse the effect of the M_w on the overall crystallinity of the samples while in the second part we will discuss the fine details of the structure as a function of M_w.

3.1. Crystallizability and molecular weight

Fig. 4 shows the experimental melting curves of the rapidly crystallized PEM samples at a heating rate of 10°C min^{-1}. As expected, by increasing M_w the maximum and the final temperatures of the endothermic peak shift towards higher temperature values. This and other details concerning the melting process will be discussed in a forthcoming publication [13]. Let us for the moment concentrate our attention on the overall enthalpy of melting as obtained by the integration of the c_p curve in the interval between 30°C and 140°C. The results are plotted on Fig. 5 in a semi-log plot as a function of M_w. A clear linear relationship is found and the evolution of ΔH with M_w can be expressed by the empirical expression (dotted line in Fig. 5).

$$\Delta H_{exp} = 273 - 66\log\left(\frac{M_w}{M_e}\right) \text{ for } M_w > M_e \quad (5)$$

where M_e is the critical entanglement molecular weight [14,15]. In order to confirm the above law, other recently published results on PEM [16] and PE fractions [17–19] have also been included in the figure. As can be seen all the data follow quite well the trend expressed by Eq. (5). The value $M_w = M_e$ marks the transition point between the Rouse regime [20] and the entanglement regime [21]. At this point there is then an abrupt change in the crystallization behaviour of the system and the enthalpy takes a value

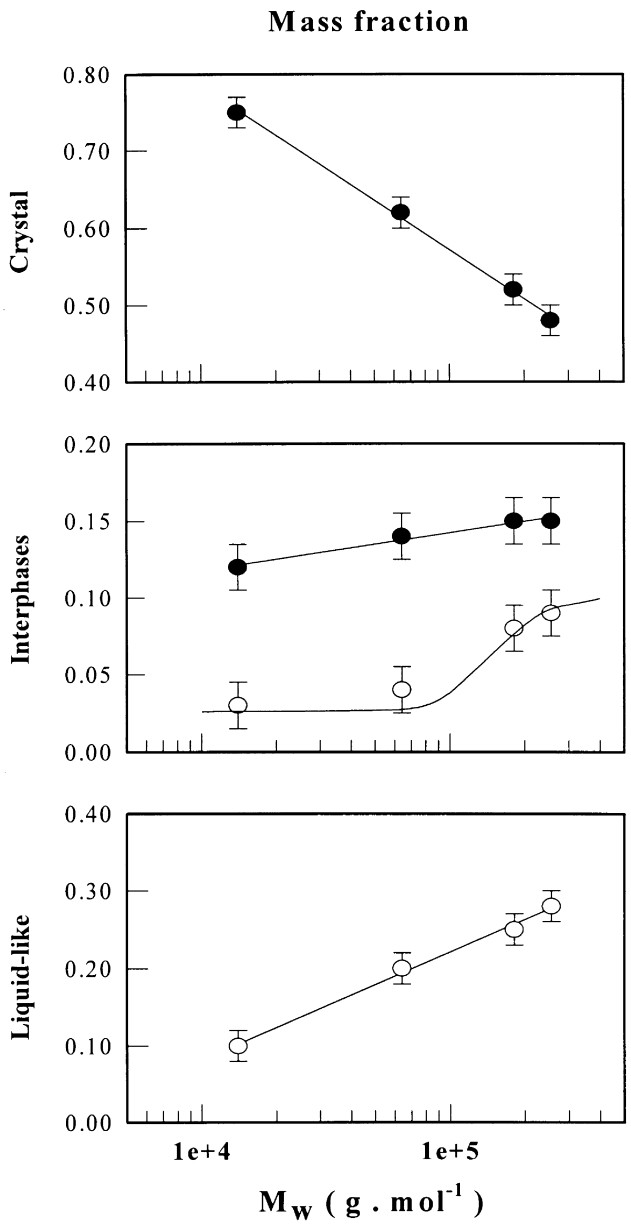

Fig. 6. Variation of the mass fraction as a function of M_w for the different phases in PEM.

close to the regular folded lamella [22]. Below M_e Eq. (5) is no longer valid. In fact, for $M_w < M_e$ a very slight tendency of ΔH to increase as M_w decreases is observable until a constant ΔH value corresponding to the extended chain crystal morphology is obtained [19].

It is worthwhile to mention that the continuous depression of the enthalpy of fusion at high M_w is quite unusual. In fact for conventional PE samples, despite their molecular weight distributions, a levelling off of the enthalpy of fusion with molecular weight has been reported [19].

3.2. The structural model

In Fig. 6 the mass fraction of the four phases as a function

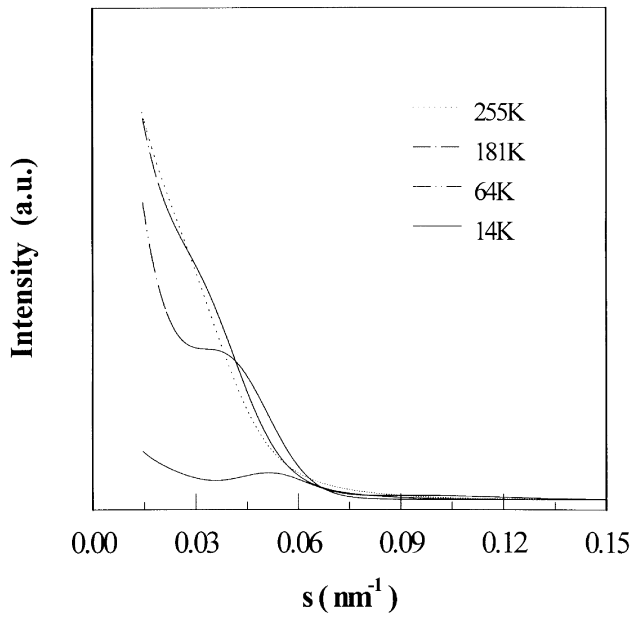

Fig. 7. Small angle X-ray scattering curves of some of the investigated PEM samples.

of the log of molecular weight has been plotted. As can be observed by increasing M_w, a clear reduction of the core crystal mass fraction is obtained. Additionally, the amount of the liquid amorphous region nearly triples its initial value from 10% to 30%. The crystalline interfacial region shows an slight increase. On the other hand, the mass fraction of the amorphous interphase shows a discontinuous behaviour with a sharp edge close to a M_w critical value of 100 K. For samples above that value a considerable amount of the chains are presumably involved in this interphase ($\alpha_{i-1} =$ 9%), while for those below the critical value a drastic decay of α_{i-1} down to 2% is detected. It is of interest to emphasize that both α_c and α_a show a linear trend with log M_w.

The X-ray experimental scattering curves in the low angle region as a function of the reciprocal vector s are plotted in Fig. 7. The samples 255 K and 181 K exhibit broad diffraction maxima overlapped to a very pronounced diffuse scattering near the zero angle. This kind of scattering curve is known to be characteristic of very high molecular weight PEs [23,24]. The diffuse scattering is indicative of density fluctuation at distances well above the average interlamellar spacing [25]. The broadening of the maxima on the other hand arises from intrinsic paracrystalline disorder of the lamellae and interlamellar region distributions. In contrast, the two low molecular weight PEs, especially the sample 14 K, exhibit well ordered and regular lamellar stacking besides to a considerably weaker diffuse scattering. The average values of the long period, L, are collected also in Table 2. As has been reported before [26], L increases with M_w.

Table 2
Macroscopic density, ρ, long period, L, and thickness of the crystal core, l_c, liquid-like, l_l, and crystalline, l_{i-c} and amorphous, l_{i-1}, interphase regions

Sample	ρ(g cm^3)	L(nm)	l_c(nm)	l_{i-c}(nm)	l_{i-1}(nm)	l_l(nm)
255 K	0.943	29.7	13.4	2.2	1.4	9.2
181 K	0.947	26.3	13.0	2.0	1.1	7.3
64 K	0.958	22.3	13.2	1.6	0.5	5.0
14 K	0.973	18.1	13.2	1.1	0.3	2.1

The thickness of each phase can be calculated from the following expression:

$$l_j = L\alpha_j \frac{\rho}{\rho_j} \tag{6}$$

where α_j and ρ_j are the mass fraction and the density of the j phase, respectively, and ρ is the average density of the sample. Let us first discuss the density value to be assigned to each phase.

The average density values ρ are collected in Table 2. The density of the core crystal ρ_c can be taken equal to 1.000 g cm^{-3} since the unit cell parameters are independent of M_w under the crystallization conditions here employed [4,27]. The density of the chains in the liquid-like amorphous regions, ρ_l, has been taken equal to 0.853 g cm^{-3} [5]. The density of the chains neither in the crystalline interphase nor in the amorphous interphase can be determined experimentally. However, indirect measurements situate the value of ρ_{i-c} around 0.96 g cm^{-3} [28]. This value sounds reasonable since the chains in the interfacial region are expected to have nearly the same conformation as in the crystal core. As ρ_{i-1} is concerned we have taken the value of 0.905 g cm^{-3} which is the average density between the crystalline interphase and the liquid-like regions. The values of the thickness of each phase calculated from Eq. (6) and using the above densities are collected in Table 2. As can be observed, l_c remains practically constant for all the samples while both the interfacial and the amorphous thickness increase with M_w.

Let us first recall the two most relevant results hitherto obtained: (a) the crystalline core is independent of molecular weight, and (b) the long period increases monotonously with M_w. Above all, the most striking result is the constancy of the value l_c with M_w. Indeed, in the relatively wide range of M_w investigated we observe no differences in the average length of the segments which cooperatively form the crystals within the experimental error of $\pm$ 1.0 nm. This value has been observed previously by other authors [26,29–31] in PE samples with very different molecular weights as well as in blends [29]. Thus, the obtained value of approximately 13.0 nm seems to be characteristic of linear PE crystallized at high undercoolings, ΔT. Let us try to offer an explanation to the above result. The limiting value of l_c could be related to the initial fold length of the secondary nucleus l_g* of the kinetics theory of Lauritzen–Hoffman (L-H) [32]. In fact, by a close inspection of the l_g* vs ΔT data of a previous work of one of us (J.M.S.) [33], one finds that there exist a plateau at high ΔT values. Actually the above mentioned result contribute at that time to develop the idea of the

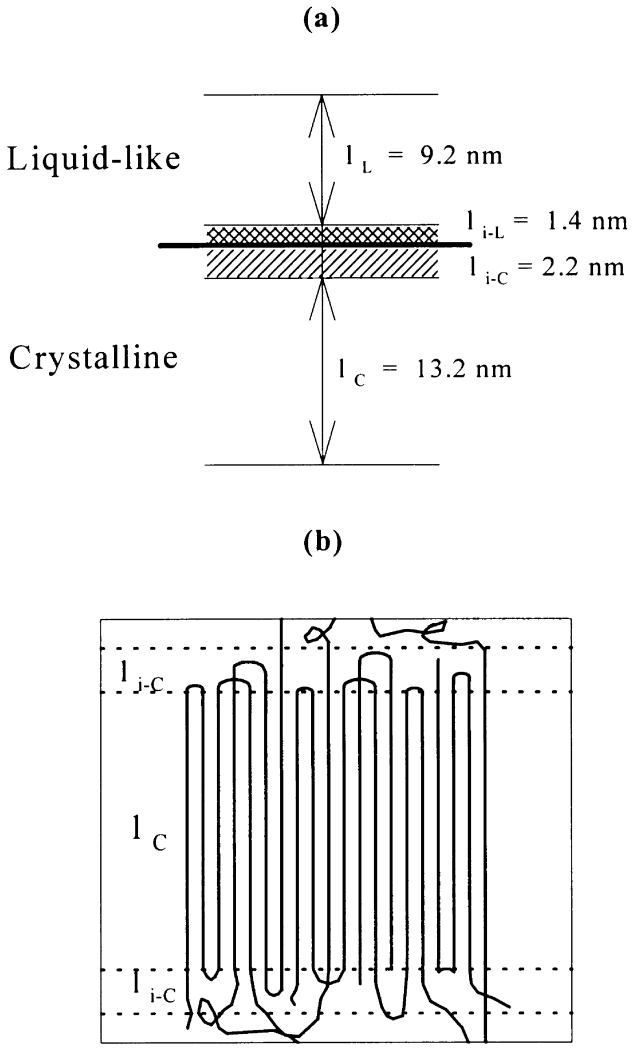

Fig. 8. Sketch of the layer structure in PEM showing comparatively the relative size of each phase.

regime III of the L-H theory [34]. It is worthwhile to mention that the values of the initial folding obtained at high ΔT using the droplets technique were precisely around the 13.0 nm that is observed in our melt-quenched samples. Let us then admit that constraint-free molecular segments of sufficient length start the crystals by nucleation into a regular folded conformation of 13.0 nm thick. This is always possible providing that the characteristic time for reeling in the segment from the melt is lower than the lateral growth rate. Taking the highest overall growth rate of $2\,ms^{-1}$ reported by Barham et al. [35], one can derive that the typical time for the deposition of three to four folds would be of the order of 10^{-5} which happens to be lower than the characteristic relaxation time of the segment involved, 10^{-3} s [36,37]. The event could occur then at multiple niches as the regime III predicts. The propagation of the growth front at each niche would be then heavily constrained by the entanglement points of the network in such a way that folding at the initial value could not be longer maintained. However, molecular segments adjacent to the initially folded nucleus could continue the lateral growth of the crystal by adopting the minimum energy conformation of the orthorhombic packing. This process implies in fact a reduction of the surface-free energy of the crystals as compared to the value predicted by the L-H theory for regular folding. The average crystal core thickness should then to be close to the initial fold length. It is of interest to recall that the characteristic entanglement length, ca. 16.0 nm for PE [14,15], is above the observed crystal core thickness and close to the maximum thickness value obtained in our samples considering both the crystal core and the interfacial region adjacent to it. The simple mechanism described above would explain the constancy of the crystal core with molecular weight.

The semi-crystalline system is assumed to consist of folded-chain lamellae. The drastic change of densities from 1 at the crystal core to 0.853 corresponding to the non-crystallized amorphous region, and consequently the required dissipation of the chains at the crystal surface cause the majority of the chains to re-enter the same crystal from which they emerge. The probability of re-entering the same crystal for the solution-growth single crystals is close to 1 while for the specimens crystallized from the melt in Regime III, this probability is severely reduced to ca. 0.7 [6]. The mechanism of chain re-entry into the lamellae has been widely investigated; however, especially for melt-crystallization process, the problem is far from being resolved. The extreme cases of the chain re-entering problem are the adjacent regular folding and the switchboard models. In the former case ideally the molecules fold back and forth with hairpin turns. On the contrary, in the switchboard model, the chains rather enter into the lamellae more or less randomly. The results from neutron scattering experiments show that even in the most favourable cases (solution-grown single crystals) only a fraction of chains can be engaged in adjacent foldings [38–40]. For dilute solution-grown crystals a better fit of the experimental results is achieved by means of a modified regular re-entry model, where the same molecule forms a new stem either after immediate re-entering or after skipping over one or two nearest-neighbour sides. Upon crystallization from the melt, the neutron scattering experiments show that a nearly random stem re-entry (some type of switchboard model) was most likely to occur [39–41]. However, as pointed out by Hoffman [7], even for melt-crystallized samples some regular folding is necessary to account for the density at the crystalline–amorphous interphase.

Let us then consider the folded-chain lamellae to be formed of a completely ordered core crystal with a thickness equal to l_c and two folding surface layers, each with a thickness equal to l_{i-c}. As first proposed by Sadler et al., the surface layer can be envisaged with the folds at different lengths of the immediate surface of the core crystal and therefore the idea of a unique fold depth should be excluded and instead a distribution of fold depths has to be brought in

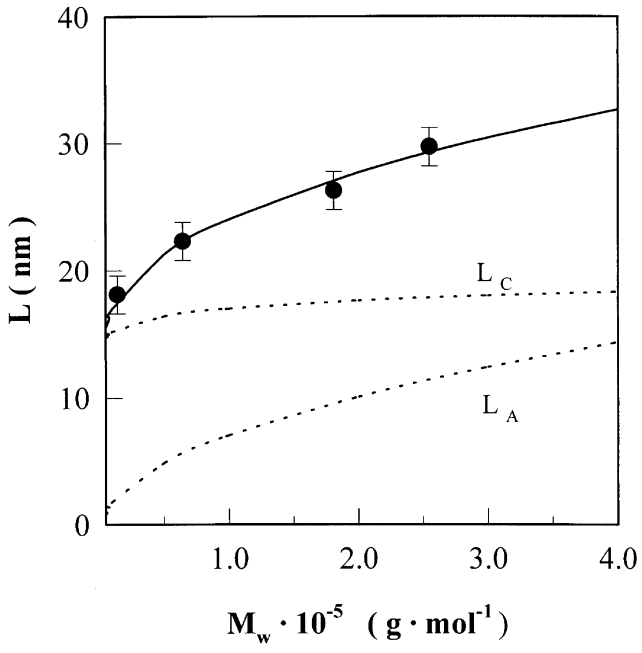

Fig. 9. Experimental long period values, symbols, of the PEM and predicted L values as a function of M_w. The predicted crystalline, (L_c) and amorphous (L_a) contributions are also shown.

mind [42]. The sketch of such a folded-chain structure is presented in Fig. 8. In fact, the rough surface layers separate the core crystal regions from the non-crystalline–amorphous layers, so we will refer to them as the 'transition layers'. The all-trans segments to some degree penetrate the transition layers more than they would in the truly amorphous regions. However, as observed in Fig. 8, in contrast to the core crystal regions, the all-trans segments in the transition layers do not present any regular lateral packing in accordance to the ideas mentioned in the introductory part of this paper. The degree of order between each folded-chain lamellae can be defined as:

$$\omega_i = \frac{l_c}{L_c} \tag{7}$$

where $L_c = l_c + 2l_{i-c}$ is the total length of the folded-chain lamellae. Here we are reminded that under rapid crystallization conditions, Regime III, l_c is constant. Obviously the maximum degree of order between the folded-chain lamellae, α_c^{max}, may be attained when the average thickness of the transition layers is minimum. This situation would correspond to a mainly regular folding mechanism, i.e. to a solution-grown lamellae with identical core crystal thickness. Based on our experimental results the following expression for ω_i as a function of the repeating units per chain, N, has been derived:

$$\omega_i = \alpha_c^{max} - k_1 \log\left(\frac{N}{N_e}\right) \tag{8}$$

In the above expression $N_c = 270$ is the critical number of repeating units between entanglements and k_1 is a constant equal to 0.093. For α_c^{max} a value close to 0.91 has been obtained. This later value is in good agreement with the observed crystallinity level of single crystals of PE grown from dilute solutions [22]. Therewith for the total length of the folded-chain lamella we can write:

$$L_c = \frac{1_c}{\alpha_c^{max} - k_1 \log\dfrac{N}{N_e}} \tag{9}$$

On the other hand, the long period would be determined by the average density of entanglements which is molecular weight dependent. So the high molecular weight sample would lead to higher long period values as is found experimentally.

In the case of polymers crystallized from the melt, Schelten et al. [43] and Crist et al. [44] found that the radius of gyration of chains in bulk material was similar to that in the molten state. This led Flory and Yoon [45] to conclude that the random entanglements in the molten state must be largely preserved and concentrated during solidification. The necessary condition for the fulfilment of the above statements is that the samples have to be severely undercooled and most surely large portions of crystallization have to take place in Regime III. At each temperature $T > T_m$, and after a period of time t, the random coils will achieve an equilibrium conformational state characteristic of that temperature. Upon rapid cooling, the crystallization takes place almost immediately, and therefore the structure of the chains is very similar to the initial state before cooling, and at least in the case of the long chains there is not enough time for the molecules to fully adopt the conformational state characteristic of the crystallization temperature.

Consequently, it is not surprising that the thickness of the amorphous layer was related to the characteristic parameters of the molecules in the molten state. For M_w higher than M_e, the molten state is described by means of an entanglement lattice, which in turn is related to the number of times that a given chain crosses a fictitious plane [15]. The number of entanglement points for a given chain is in turn is proportional to the square root of the number of repeating units of the gaussian chains [46]. This is due to the fact that the volume occupied by a chain of N-monomers is proportional to the radius of gyration of the gaussian chain to the third, $R_g^3 \propto N^{3/2}$, while the cross section of an arbitrary plane is proportional to $R_g^2 \propto N$.. Again based on our experimental results the following expression for L which is the sum of both the liquid-like and amorphous interphase layers, can be derived:

$$L_a = k_2\sqrt{\frac{N}{N_e} - 1} \tag{10}$$

where k_2 is a constant equal to 1.40.

In the linear model it is assumed that the lamellar stacks are effectively of infinite lateral size, so that only the one dimensional variation of electron densities normal to the

lamellar planes accounts for scattering. Under these assumptions all the amorphous material have to be located between the lamellar crystals. The applicability of this model to melt-crystallized linear PE samples has been verified recently [47]. Then the long spacing L is just the sum of both the folded-chain and the amorphous layer lengths, i.e. $L_c = L_a + L_a$. Combining Eqs. (9) and (10), we can rewrite the following expression for the long period:

$$L = \frac{l_c}{a_c^{max} - k_1 \log \frac{N}{N_e}} + k_2 \sqrt{\frac{N}{N_e} - 1} \quad (11)$$

In Fig. 9 the experimental values of the long period as a function of $\log(M_w)$ are plotted. The solid curve in this figure is calculated from Eq. (11). The contributions of the folded-chain length, L_f, and amorphous layers, L_a, are drawn separately.

4. Conclusions

Polymerization based on the new generation of metallocene catalysis results in a better design of the polyethylene architecture as compared to the traditional Ziegler–Natta products. The linear molecules, free of short chain branching and with an almost symmetrical distribution, exhibit a remarkable homogeneous behaviour upon rapid crystallization from the melt. The crystallizability of this PEM is strictly controlled by the length of the molecule which defines the long period of the structure. The crystal core remains identical with molecular weight and the increasing value of the disordered regions with M_w yields a monotonous decrease of the crystallinity of the system. Various semi-empirical equations are derived from the experimental data as a function of a single parameter: the molecular weight.

Acknowledgements

Thanks are due to CAM (grant I + D 058/94) for the support of this investigation. The authors also acknowledge Repsol S.A. for the permission to publish some of the data, and A.A.A. thanks CICYT and Repsol S.A. for the tenure of a PETRI fellowship.

References

[1] Kaminsky W, Miri M, Sinn H, Woldt R. Macromol Chem Rapid Commun 1983;4:417.
[2] Flory PJ. Principles of polymer chemistry. Ithaca, NY: Cornell University Press, 1986.
[3] Klug HP, Alexander L. X-ray diffraction procedures for polycrystalline and amorphous materials. New York: Wiley, 1974.
[4] Bunn CW. Trans Faraday Soc 1939;35:482.
[5] Chiang R, Flory PJ. J Am Chem Soc 1961;83:2857.
[6] Flory PJ, Yoon DY, Dill KA. Macromolecules 1984;17:862.
[7] Di Marzio EA, Guttman CM, Hoffman JD. Faraday Discuss Chem Soc 1979;68:177–297.
[8] Strobl G, Hagedron W. J Polym Sci Polym Phys 1978;16:1181.
[9] Mutter R, Stille W, Strobl G. J Polym Sci Polym Phys 1993;31:99.
[10] Cheng J, Fone M, Reddy VN, Schwartz KB, Fischer HP, Wunderlich B. J Polym Sci Polym Phys 1994;32:2683.
[11] Kaminsky W, Hahnse H, Ulper K, Woldt R. US Patent 4542199, 1985.
[12] Alizadeh Azimi A, Muñoz-Escalona A, Martínez-Salazar J. Polymer 1997;38:1207.
[13] Muñoz-Escalona A, Alizadeh Azimi A, Martínez-Salazar J. In preparation.
[14] Carella JM, Graessley WW, Fetters LJ. Macromolecules 1984;17:2775.
[15] Wool R. Macromolecules 1993;26:1564.
[16] Eskelinen M, Seppälä JV. Eur Polym J 1996;32:331.
[17] Hedenqvist M. PhD thesis, University of Stockholm, 1995.
[18] Stack GM, Mandelkern L, Voigt-Martin IG. Macromolecules 1984;17:321.
[19] Mandelkern L, Stack GM. Macromolecules 1984;17:871.
[20] Rouse PE. J Chem Phys 1953;21:1272.
[21] De Gennes PG. Scaling concepts in polymer physics. Ithaca, NY: Cornell University Press, 1979.
[22] Wunderlich B. Macromolecular physics, vol. 3. New York: Academic Press, 1980.
[23] Lee YD, Philips PJ, Lin JS. J Polym Sci Polym Phys 1991;29:1235.
[24] Bellare A, Schnablegger H, Cohen RE. Macromolecules 1995;28:7585.
[25] Hosemann R, Bagchi SN. Direct analysis of diffraction by matter. Amsterdam: North Holland, 1962.
[26] Souffaché ER, Rault J. Macromolecules 1989;22:3581.
[27] Alizadeh Azimi A. PhD thesis, University Autonoma of Madrid, 1997.
[28] Földes E, Keresztury G, Iring M, Tüdos F. Agnew Makromol Chem 1991;187:87.
[29] Mandelkern L, Alamo RG, Kennedy MA. Macromolecules 1990;23:4721.
[30] Mandelkern L, McLaughlin KW, Alamo RG. Macromolecules 1992;25:1440.
[31] Capaccio G, Wilding MA, Ward IM. J Polym Sci Polym Phys 1981;19:1489.
[32] Hoffman J, Davis GT, Lauritzen JI. Treatise on solid state chemistry, vol. 3. New York: De Plenum Press, 1976.
[33] Barham PJ, Chivers RA, Keller A, Martínez-Salazar J, Organ SJ. J Mater Sci Lett 1985;20:1625.
[34] Hoffman JD. Polymer 1983;24:3.
[35] Barham PJ, Jarvis DA, Keller A. J Polym Sci Polym Phys 1982;20:1733.
[36] Klein J, Ball RC. Discuss Faraday Chem Soc 1979;68:198.
[37] Klein J. Encyclopedia of polymer science and engineering, vol. 9. New York: Wiley, 1987.
[38] Keller A. Faraday Discuss Chem Soc 1979;68:145.
[39] Sadler DM, Keller A. Macromolecules 1977;10:1128.
[40] Sadler DM, Keller A. Science 1979;203:263.
[41] Yoon DY, Flory PJ. Faraday Discuss Chem Soc 1979;68:289.
[42] Sadler DM. Farday Discuss Chem Soc 1979;68:106.
[43] Schelten J, Wignal GD, Ballard DGH. Polymer 1974;15:682.
[44] Crist B, Graessley W, Wignal GD. Polymer 1982;23:1561.
[45] Flory PJ, Yoon DY. Nature 1978;272:226.
[46] Holl B, Heise B, Killian HG. Colloid Polym Sci 1983;261:978.
[47] Stribeck N, Alamo RG, Mandelkern L, Zachmann HG. Macromolecules 1995;28:5029.